Engineering Geology 264 (2020) 105383

Contents lists available at ScienceDirect

Engineering Geology

journal homepage: www.elsevier.com/locate/enggeo

Mechanical behavior of GMZ bentonite pellet mixtures over a wide suction range

Zhao Zhang[a], Wei-Min Ye[a,b,*], Zhang-Rong Liu[a], Qiong Wang[a,b], Yu-Jun Cui[a,c]

[a] Department of Geotechnical Engineering, College of Civil Engineering, Tongji University, Shanghai 200092, China
[b] Key Laboratory of Geotechnical and Underground Engineering of Ministry of Education, Tongji University, Shanghai 200092, China
[c] Laboratoire Navier, Ecole des Ponts ParisTech, France

ARTICLE INFO

Keywords:
GMZ bentonite pellet
Suction
Swelling pressure
Swelling deformation
Compression

ABSTRACT

High-density bentonite pellet mixtures have been proposed as candidate materials for filling technological voids in the deep geological disposal repository of high-level radioactive waste (HLW). Water vapour transfer plays a major role in the function formation of the unsaturated engineering barrier system, due to the existing high thermal gradients generated by the decay heat released from the canister. In this work, series of suction controlled swelling pressure tests, swelling deformation tests and compression tests were conducted on GMZ bentonite pellet mixtures. Results show that, for the specimen hydrated by the vapour equilibrium technique, no collapse was observed on the evolution curve of swelling pressure. However, for that wetted by the osmotic technique, a collapse of swelling pressure was observed after the first peak value. For specimens hydrated with suction-control, a collapse on the evolution curve of swelling strain was only observed under high vertical stresses. In addition, the unloading curves of specimens exhibited a linearity at the high suction stage and a bi-linearity at the low suction stage. The swelling pressure determined by the swell-consolidation method was higher than that determined by the constant-volume method.

1. Introduction

The deep geological disposal of high-level radioactive waste (HLW) has been recognized as a safe solution to isolate the waste from the biosphere (SKB, 2007; Posiva, 2010). According to the conceptual design of a "multi-barrier system" in the repository, compacted bentonite (in blocks) is often chosen as buffer/backfill materials emplaced between the canister and the host rock due to its high swelling capacity, low permeability and strong adsorption property (Komine, 2004; Ye et al., 2010). Studies indicate that technological gaps among bentonite blocks and between blocks and host rock /canisters will be unavoidably encountered during the installation of compacted bentonite blocks (Dixon et al., 2011; Wang et al., 2013; Marjavaara et al., 2014). High-density bentonite pellets have been proposed as a promising material for filling these technological gaps, due to easier engineering manipulation, less compaction effort and more suitable for backfilling irregularly shaped spaces (Imbert and Villar, 2006; Molinero-Guerra et al., 2017).

Practically, once installed in the repository, bentonite pellets will be subjected to the infiltration of ground water and the mechanical loading from the geological barrier. More importantly, during the following long-term operation of the repository, due to the low permeability of the engineering barrier, the bentonite pellet mixtures might be in an unsaturated state for a long time. During this time period, water vapour transfer will play a major role in the function formation of the engineering barrier system, due to the existing high thermal gradients generated by the decay heat released from the canister (Romero et al., 2005; Villar and Lloret, 2004; Cui et al., 2011). With the water vapour infiltrated, bentonite pellets will swell and fill in the surrounding spaces, and then, the swollen pellets gradually turn to be consolidated by the swelling pressure generated by the surrounding compacted bentonite blocks in the repository (Sugita et al., 2003). Therefore, it is necessary to get insights into swelling and compressibility properties of bentonite pellet mixtures during the whole process of water vapour transfer for assessing the overall function of the engineering barrier system.

In the last few decades, studies have been performed focusing on investigations of mechanical behaviors of granular bentonite materials. Imbert and Villar (2006) carried out a series of infiltration tests on FoCa Clay pellet/powder (50/50) mixtures and concluded that the swelling pressure curves were characterized by a "double-peak" shape. Alonso et al. (2011) investigated hydro-mechanical behaviors of compacted

* Corresponding author at: Department of Geotechnical Engineering, College of Civil Engineering, Tongji University, Shanghai 200092, China.
E-mail address: ye_tju@tongji.edu.cn (W.-M. Ye).

https://doi.org/10.1016/j.enggeo.2019.105383
Received 25 April 2019; Received in revised form 15 September 2019; Accepted 28 October 2019
Available online 31 October 2019
0013-7952/

FEBEX bentonite pellet mixtures and concluded that the hydraulic and mechanical properties of this material were dependent of its interactions between different structural levels. Hoffmann et al. (2007) carried out MIP tests on compacted FEBEX pellet mixtures at different dry densities and found that this material was characterized by a multiple-porosity network, including intra-aggregate pores, inter-aggregate pores and inter-pellet pores. During the wetting process, the expansion of pellets induced the progressive blockage of large-pores (inter-pellet pores), leading to a significant reduction of permeability and a possible collapse of granular structure (Van Geet et al., 2005; Molinero-Guerra et al., 2018).

However, most of these previously conducted wettings of bentonite pellet mixtures were performed by injecting liquid water. The volumetric behaviors of the granular materials obtained were quite different to those tested with infiltration of water vapor, due to the inconsistency of macrostructural and microstructural water potentials (Hoffmann et al., 2006; Alonso et al., 2011). Moreover, compared to that of compacted bentonite powder, the mechanical behavior of the granular materials (pellet mixtures) appears to be more complex, due to the possible rearrangements or crush of pellets during the wetting process or under vertical loads at the high suction stage (Pestana and Whittle, 1995; Molinero-Guerra et al., 2018).

Chinese program for HLW disposal was launched in the middle of 1980s. Beishan in Gansu Province has been selected as the preferred construction site for the first repository to be constructed. Gaomiaozi (GMZ) bentonite has been proposed as the first choice of buffer/backfill materials (Ye et al., 2010).

In this work, suction controlled step-by-step swelling pressure tests were firstly performed on GMZ bentonite pellet mixtures to investigate the development of swelling pressure with hydration of water vapour. Then, suction controlled swelling deformation tests were conducted under constant-loading conditions. Influences of vertical loads and suction on swelling properties were analyzed. Finally, suction-controlled compression tests were carried out to investigate the compressibility properties of specimens at different suctions. Results obtained are of great importance for the design of engineering barrier system and safety assessments of Chinese deep geological repository involving this granular material.

2. Materials

2.1. GMZ bentonite and its pellet fabrication

The GMZ bentonite tested in this study is extracted from Inner Mongolia of China, 300 km northwest from Beijing. The XRD pattern of GMZ bentonite powder indicates that the dominant mineral is montmorillonite (Wen, 2006). Some basic properties of GMZ bentonite are listed in Table 1. The initial water content of GMZ bentonite powder is 10.60%, corresponding to a total suction 113 MPa.

For the pellet fabrication, GMZ bentonite powder was firstly compacted into high-density blocks (ρ_d = 1.94 ~ 1.96 Mg/m^3), and then crushed into pellets by a jaw crusher. The detailed fabrication procedure can be found elsewhere (Zhang et al., 2018). Finally, the crushed pellets were sieved into different groups (< 0.075 mm, 0.075 ~ 0.25 mm, 0.25 ~ 0.5 mm, 0.5 ~ 0.9 mm, 0.9 ~ 2 mm, 2 ~ 5 mm and 5 ~ 7 mm) and controlled to a total suction of 113 MPa in a hermetic container at 20 °C.

Table 1
Basic properties of GMZ bentonite (Wen, 2006).

Property	Description
Specific gravity of soil grain	2.66
pH	8.68–9.86
Liquid limit(%)	276
Plastic limit(%)	37
Total specific surface area/(m^2 g^{-1})	570
Cation exchange capacity/(mmol g^{-1})	0.7730
Main exchanged cation/(mmol g^{-1})	Na^+(0.4336),Ca^{2+}(0.2914) Mg^{2+}(0.1233),K^+(0.0251)
Main minerals	Montmorillonite (75.4%) Quartz (11.7%) Feldspar (4.3%) Cristobalite (7.3%)

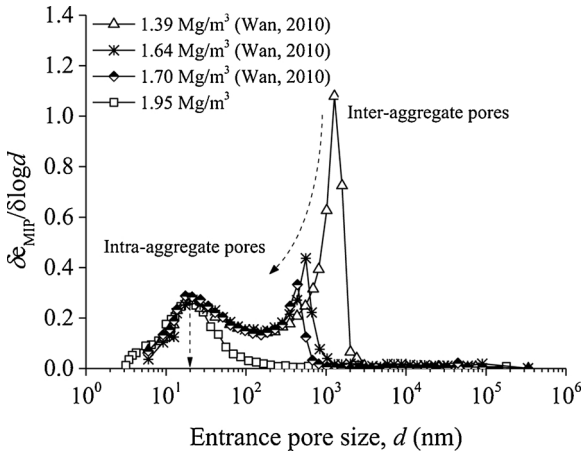

Fig. 1. Pore size distribution curves of compacted GMZ bentonite.

The pore structures of compacted pure bentonite are commonly composed of two levels of pores, including intra-aggregate pores (micro-pores) and inter-aggregate pores (macro-pores). The intra-aggregate pores correspond to active clay minerals with prevailing physico-chemical effects, while the inter-aggregate pores are responsible for major structural rearrangements (Gens and Alonso, 1992; Lloret et al., 2003). The pore size distribution curves of compacted GMZ bentonite specimens with different dry densities are shown in Fig. 1. A typical bimodal porosity can be observed from curves of three specimens with dry densities of 1.39 Mg/m^3, 1.64 Mg/m^3 and 1.70 Mg/m^3. Intra-aggregate and inter-aggregate pores can be distinguished from the curves, as compaction loads mainly affect the inter-aggregate pores (Lloret et al., 2003; Lloret and Villar, 2007). Moreover, when compacted to a dry density of 1.95 Mg/m^3, the pore size distribution curve of compacted pure bentonite (or a single pellet) shows a unimodal pattern and the inter-aggregate pores almost disappear.

2.2. Specimen preparation

Zhang et al. (2018) once conducted packing density tests on GMZ bentonite pellet mixtures for investigation of particle size distribution (PSD) effects on packing dry density. Experimental results indicated that, according to Eq. (1), when q = 0.4 and d_{max} = 7 mm, the highest packing dry density of specimen could be obtained with a corresponding PSD curve shown in Fig. 2.

$$P_t = (d/d_{max})^q \quad (1)$$

where, P_t is the fraction of the total solid with a particle size smaller than d, d_{max} is the maximum particle size in the mixture, q is the distribution modulus with a value between 0 and 1.

According to the PSD curve in Fig. 2, two groups of the pellet mixtures were prepared, including the coarse group (> 2 mm) and the fine one (< 2 mm). Then, according to the target dry density (1.45 Mg/m^3) and the designed dimension (50 mm in diameter and 35 mm in height) for the specimens of pellet mixtures to be compacted, pellets in two groups were weighed and alternatively put into the container in three layers. After that, the container with specimen was vibrated for 180 s using a vibrating table (Zhang et al., 2018). Finally, the specimen was statically compacted to a target height (35 mm) at a rate of 0.2 mm/min, corresponding to its target dry density.

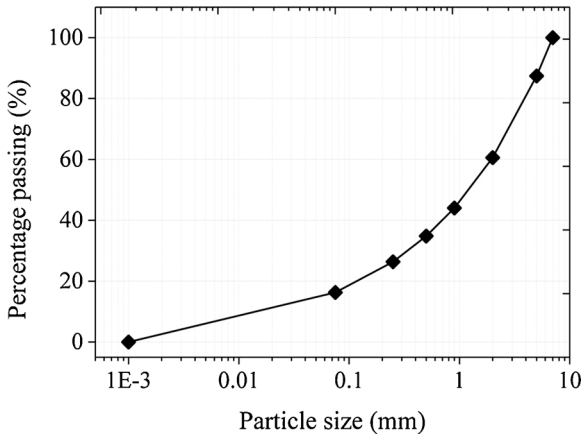

Fig. 2. Particle size distribution curve of the pellet mixture.

For this pellet mixture specimen prepared in this work, a pore structure of bimodal porosity with intra-pellet (aggregate) pores (microstructural level) and inter-pellet pores (macrostructural level) can be identified (Hoffmann et al., 2007; Molinero-Guerra et al., 2017).

3. Experimental investigation

3.1. Swelling pressure tests with suction control

3.1.1. Apparatus

For conducting suction-controlled swelling pressure tests under constant-volume conditions, the test device designed by Zhu et al. (2013) was employed in this work. It mainly includes three parts: (1) a stainless steel cell, (2) a data logging system and (3) a suction-controlled hydration system (Fig. 3). The cylindrical cell is made of 316 stainless steel and has an inner space of 50 mm in diameter (with a 30 mm thick wall) and 60 mm in height for holding the specimen sandwiched between two porous stones. Two inlets (outlets) are designed at the bottom part of the cell for circulating vapor/liquids. A stainless piston with a load transducer on its top is employed and the system is fixed by using four screws. The data logging system is used for recording the swelling pressure of the specimen. Meanwhile, the vapour equilibrium technique (VET) (Fig. 3a) and osmotic technique (OT) (Fig. 3b) are employed for high suction (> 4.2 MPa) and low suction (< 4.2 MPa) control, respectively.

The VET method was widely adopted by researchers for controlling total suction in unsaturated soils (Delage et al., 1998; Romero, 2003; Tang and Cui, 2007; Ye et al., 2009, 2012). For conducting suction-control tests using the VET technique, the humid vapor of saturated salt solutions contained in a separated bottle is circulated using a pneumatic pump to ensure the efficient vapor hydration of the specimen (Fig. 3a). In this study, saturated salt solutions of K_2CO_3, NaCl, KNO_3 and K_2SO_4 corresponding to suctions of 113 MPa, 38 MPa, 9 MPa and 4.2 MPa at 20 °C were employed.

Simultaneously, the OT method is also a widely accepted technique for suction-control in unsaturated soil mechanics (Delage et al., 1998; Blatz et al., 2008). For conducting suction-controlled tests using the OT technique, the semi-permeable membrane is placed over the porous stone, with a cylindrical sample resting directly on it. An osmotic solution containing large sized polyethylene glycol (PEG) is circulated behind the semi-permeable membrane. Since the membrane is permeable to water and ions but impermeable to large sized PEG molecules, the suction is applied on the sample through the membrane. In the osmotic system, the controlled suction of specimen increased with the concentration of PEG solutions and the relationship between them was given by Delage et al. (1998).

3.1.2. Test procedures

In this work, two specimens were submitted to conduct suction-controlled swelling pressure tests. In the specimen SP-01, three suctions 38 MPa, 9 MPa and 4.2 MPa were successively applied using the vapour equilibrium technique. Then, the specimen was directly saturated by infiltrating distilled water. In the test SP-02, the specimen was suction-controlled to suctions 0.92 MPa, 0.17 MPa and 0 MPa using the osmotic technique with corresponding concentrations of the PEG 20,000 solutions.

All the tests were conducted at an ambient temperature 20 ± 0.5℃.

3.2. Swelling deformation tests with suction and vertical stress control

The oedometer cell employed for conducting swelling deformation tests under suction and vertical stress control has an inner space of 50 mm in diameter and 60 mm in height. A piston is employed for applying the vertical stress on the specimens. A strain gauge with a precision of 1 μm is fixed on the loading piston for monitoring the vertical deformation. Similar to suction-controlled swelling pressure tests, the vapour equilibrium technique and the osmotic technique are respectively designed for fulfilling suction-control. To apply zero suction, distilled water is circulated under the bottom of the specimens.

In order to investigate suction and loading effects on swelling deformation of specimens, nine specimens with a dimension of 50 mm in diameter and 35 mm in height, as well as a target dry density of 1.45 Mg/m^3 are respectively prepared. Specifications of swelling deformation tests conducted are shown in Table 2.

3.3. Compression tests with suction control

For specimens SD-01, SD-02, SD-06 and SD-07, once the swelling deformation tests were finished, suction controlled compression tests were performed. Meanwhile, one additional specimen (SCC-01) with an initial suction 113 MPa was also submitted to the compression test. The experimental setup with a double-arm level loading system developed by Ye et al. (2012) was employed for conducting compression tests in this work. A maximum load of 80 MPa can be safely applied on the

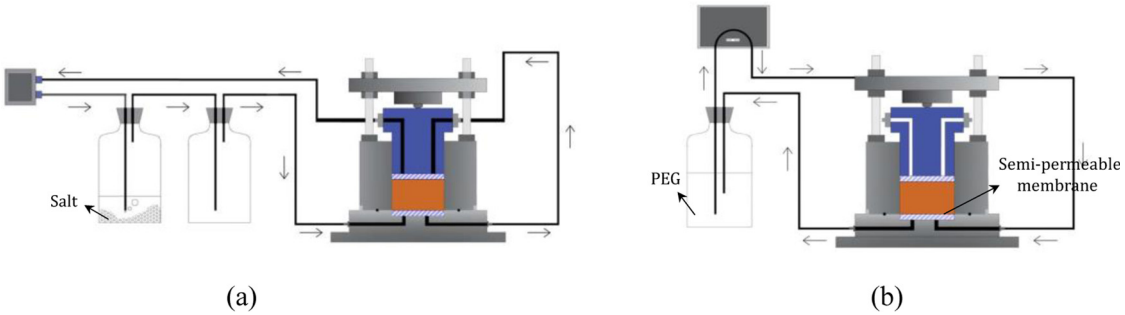

Fig. 3. Suction-controlled hydration system by (a) VET; (b) OT.

Table 2
Specifications of swelling deformation tests conducted.

Specimen	Initial dry density (Mg/m^3)	Vertical pressure (MPa)	Controlled suction (MPa)	Suction control technique
SD-01	1.45	0.1	113→38	VET
SD-02	1.45	0.1	113→9	VET
SD-03	1.45	0.1	113→4.2	VET
SD-04	1.45	0.1	113→0.81	OT
SD-05	1.45	0.1	113→0.39	OT
SD-06	1.45	0.1	113→0.1	OT
SD-07	1.45	0.1	113→0	WC
SD-08	1.45	0.4	113→39→9 →4.2→0	VET + WC
SD-09	1.45	0.8	113→39→9 →4.2→0	VET + WC

SD: swelling deformation test, WC: water circulation, VET: the vapour equilibrium technique, OT: the osmotic technique.

specimen with a diameter of 50 mm. The strain gauge employed in compression tests is the same as that used in the swelling deformation tests. A volumetric strain rate of less than 0.025%/day was adopted as the cut-off criterion of equalization at each loading step (Romero et al., 2003). Suction controlled techniques and oedometer cells on the experimental setup are the same as those in swelling deformation tests.

4. Results

4.1. Swelling pressure

Evolutions of swelling pressure for specimens SP-01 and SP-02 are presented in Fig. 4. The evolution curve of the specimen SP-01 shows that an apparent increase in swelling pressure can be observed while suction decreases from its initial value 113 MPa to 38 MPa. Swelling pressure rapidly increases to 0.31 MPa (t = 115 h) with an approximately constant rate at the initial stage, followed by a gradual decrease in the increasing rate, and eventually reaches a stable value 0.436 MPa at suction 38 MPa. With further reduction of suction, a slight increase in swelling pressure is recorded for 0.462 MPa at suction 9 MPa and 0.465 MPa at suction 4.2 MPa, respectively. Finally, with the injection of deionized water, swelling pressure immediately increases and ultimately reaches an equilibrium value of 0.97 MPa.

Meanwhile, the evolution of swelling pressure recorded for specimen SP-02 shows a similar “double-peak” phenomenon as suction reduces from its initial value 113 MPa to 0.92 MPa. The swelling pressure increases rapidly and reaches its first peak value 0.45 MPa (t = 87 h), followed by an intermediate phase where swelling pressure decreases to 0.43 MPa (t = 210 h). After that, swelling pressure

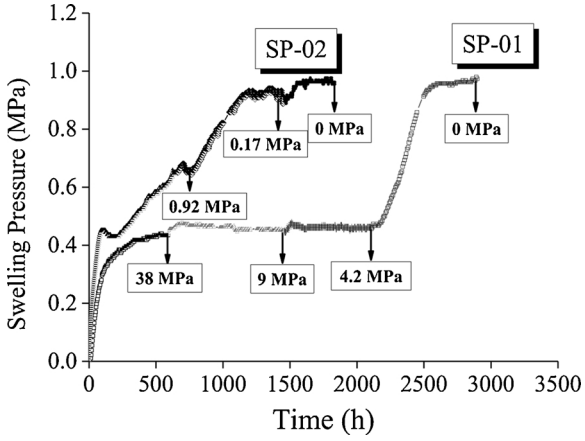

Fig. 4. Swelling pressure evolutions of specimens SP-01 and SP-02.

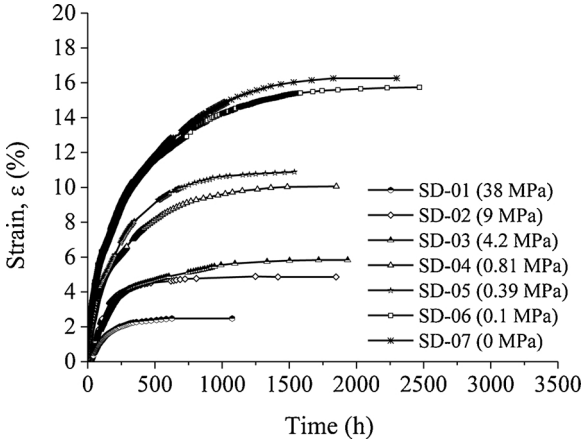

Fig. 5. Swelling strain evolutions of specimens (SD-01 to SD-07).

increases again and finally reaches the equilibrium value 0.68 MPa at suction 0.92 MPa. As suction further reduces to 0.17 MPa, swelling pressure continuously increases to an equilibrium value of 0.91 MPa. When the specimen is wetted by injecting deionized water, swelling pressure slightly increases from 0.91 MPa to 0.97 MPa. Furthermore, although two specimens are hydrated by two different techniques, the first peak values and the final ones of the swelling pressure are similar.

4.2. Swelling deformation

Evolutions of swelling strains with time for specimens SD-01 to SD-07 are presented in Fig. 5. Swelling strains monotonously increase for all the specimens with a quick increase at the initial stage and then gradually turn to be stabilized. The final swelling strains of specimens increase with suction decreasing. Evolutions of the final swelling strains with suction are presented in Fig. 6. Observation shows that, when suction decreases from its initial value 113 MPa to 4.2 MPa, swelling strain correspondingly increases to 5.8%. As suction further decreases to be lower than 4.2 MPa, more than 60% of the total swelling strain can be recorded.

Fig. 7 shows the changes of void ratio with time for specimens SD-08 and SD-09. It can be observed that as suction decreases from 113 MPa to 4.2 MPa, the void ratio of specimen SD-08 only increases from 0.807 to 0.833. However, when suction continuously decreases to zero by injecting distilled water, its void ratio significantly increases and eventually reaches its final value 0.905. For the specimen SD-09, as suction decreases from its initial value (113 MPa) to 38 MPa, a collapse of specimen is observed with void ratio correspondingly decreasing

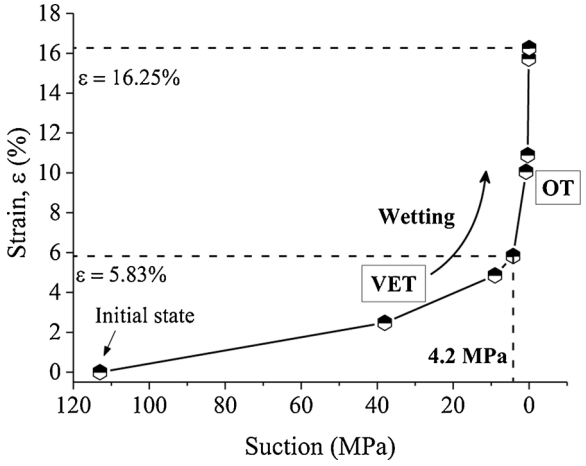

Fig. 6. Final swelling strains of specimens at different suctions.

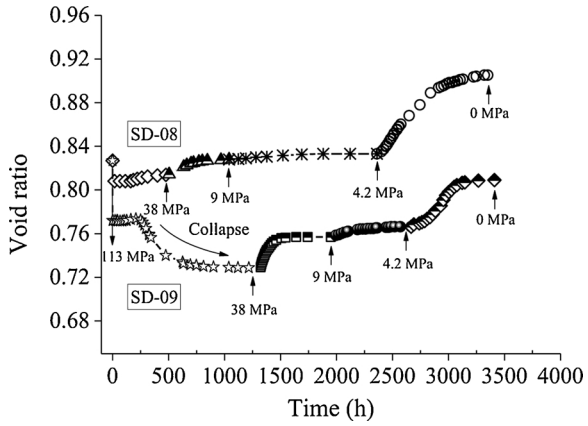

Fig. 7. Void ratio evolutions with time for specimens SD-08 and SD-09.

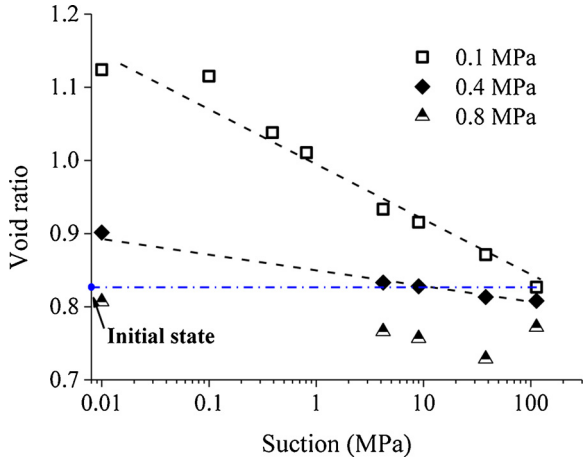

Fig. 8. Changes of void ratios with suction under different vertical loads.

from 0.773 to 0.729. Then, with the further decrease of suction, its void ratio continuously increases and eventually reaches 0.810 at suction 0 MPa. In addition, changes of void ratios with suction for specimens under different vertical stresses are presented in Fig. 8. It is observed that the expansions of specimens tested are influenced by the vertical stresses and this influence appears to be more significant at low suction stage.

4.3. Compressibility

Measured compression curves for specimens tested at different suctions were presented in Fig. 9. At the high suction stage, compression curves are characterized by an initial linear part with low compressibility (the pseudo-elastic domain), followed by a second part with higher compressibility (the plastic domain). The unloading curves at the third part exhibit the same trend as the initial loading part (the elastic domain) for specimens SCC-01 (113 MPa), SD-01 (38 MPa) and SD-02 (9 MPa). It appears that the slopes of the unloading curves are independent of suction at the high suction stage. However, for specimens tested under low suctions (SD-06 and SD-07), the unloading path confirms a nearly bi-linear curve with a small slope beyond the threshold stress σ_A and σ_C (Fig. 9b) and a large slope lower than σ_A and σ_C. Meanwhile, according to the definition of swell-consolidation method, the swelling pressure can be obtained (P_s = 2.87 MPa) from the compression curve of specimen SD-07 (Point B).

Evolutions of preconsolidation pressures with suction for specimens tested in this work and compacted GMZ pure bentonite specimens in Ye et al. (2012) were shown in Fig. 10. Fig. 10 show that a good coincidence between the preconsolidation pressures of specimens tested in this work and those of the compacted pure bentonite specimens in Ye et al. (2012) can be observed at zero-suction. However, the preconsolidation pressures of compacted pure bentonite obviously increase with the increase of suction, but this phenomenon is not clear for that of the bentonite pellet mixtures. Furthermore, Fig. 11 shows variations of the compressibility parameters λ(s) with suction. It can be deduced that the material stiffness decreases with the reduction of suction.

5. Discussion

5.1. Swelling properties

5.1.1. Hydration of bentonite

It is commonly recognized that swelling of bentonite upon hydration is closely related to the hydration of smectites. Studies revealed that, for dry smectites, hydration initially occurred on the mineral surface and around the exchangeable cations in the interlayer spaces of the clay particles (Mooney et al., 1952), i.e., the crystalline swelling (Van Olphen, 1977). As suction gradually decreases from a high value, the hydration of compacted smectite (MX-80 bentonite) specimens is governed by the progressively emplacement of one layer (s = 50 MPa), two layers (7 MPa < s < 50 MPa), three layers (s < 7 MPa) or four layers (s < 0.1 MPa) of water molecules along the surface of the unit clay layers within the particle, respectively (Saiyouri et al., 2004). Meanwhile, the number of clay layers per particle also decreases (the subdivision of particle), resulting in the generation of many thinner particles (Saiyouri et al., 2000). At the low suction state, water in inter-particle pores and the inter-particle distance significantly increase with decreasing suction. This process is commonly called the osmotic swelling, which is mainly driven by the repulsion between the diffuse double layers (DDL) (Massat et al., 2016).

5.1.2. Swelling pressure of GMZ bentonite pellet mixture

The swelling properties of bentonite pellet mixture are mainly dependent on two concurrent phenomena: the expansion of bentonite pellet upon hydration and the interactions between macro- and micro-pore structures (Alonso et al., 2011). The hydration process is dominated by the crystalline swelling or the osmotic swelling depending on the hydration degree, resulting in the swelling of bentonite pellets. Under constant-volume conditions, the swelling of pellets upon hydration causes the increase of inter-pellet force. Meanwhile, the collapse of granular structure may occur due to the rearrangement or the weakness of bentonite pellets upon hydration (Molinero-Guerra et al., 2018).

For the specimen hydrated in a step-by-step way with suction-control using the vapour equilibrium technique, a rapid increase in swelling pressure was observed while suction decreased from 113 MPa to 38 MPa (SP-01 in Fig. 4). During this process, a strong adsorption of the first two water molecule layers might occur inside the bentonite pellet (Saiyouri et al., 2004). The swelling of pellet was dominated by the crystalline swelling and the stiffness of pellets was still high. Consequently, the hydration leads to a significant increase in inter-pellet force. As suction continuously decreased to 9 MPa, and then, 4.2 MPa, insignificant changes of swelling pressure with time were observed. This phenomenon could be related to the combined interaction between the expansion of bentonite pellets and the collapse of granular structure. In fact, during this process, the stiffness of pellets significantly decreased due to the adsorption of the weak third layer of water molecular and the subdivision of clay particles (Darde et al., 2018). The specimen experienced collapse of granular structure under the swelling pressure. Finally, when the specimen was wetted by injecting liquid water, swelling pressure rapidly increased again due to the osmotic swelling.

Meanwhile, for the specimen hydrated using the osmotic technique (SP-02), the evolution curve of swelling pressure with time exhibits a “double-peak” shaped phenomenon as suction decreased from 113 MPa

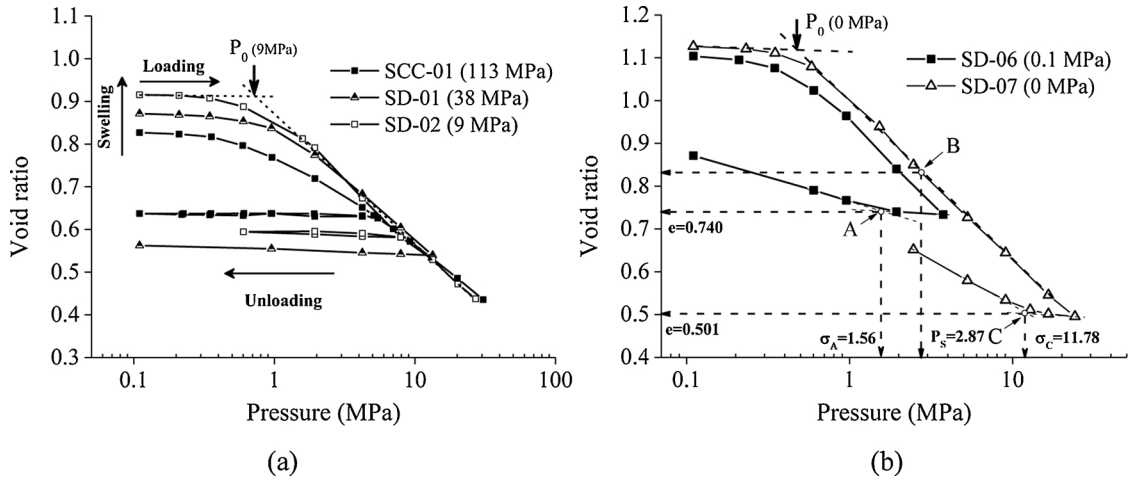

Fig. 9. Compression curves of specimens in (a) high suction and in (b) low suction.

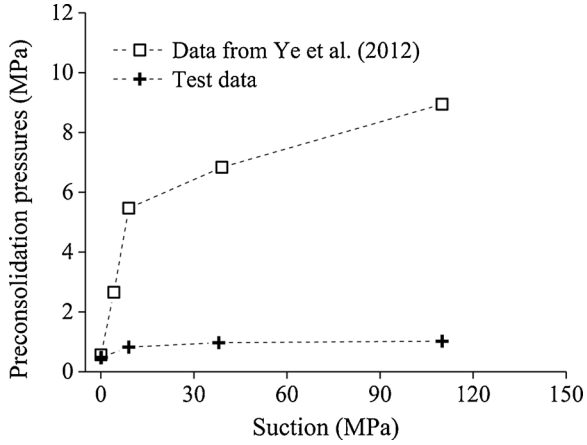

Fig. 10. Changes of preconsolidation pressures with suction.

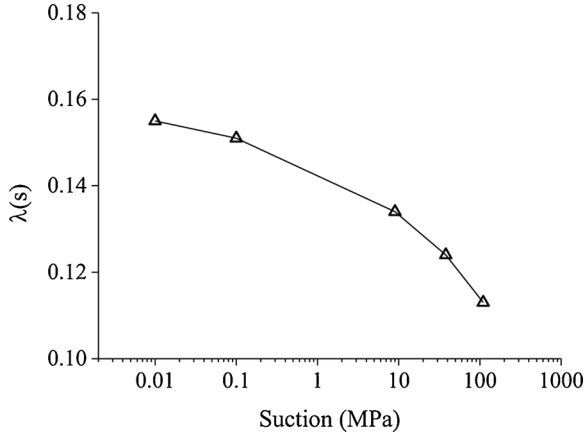

Fig. 11. Variations of compressibility parameter (λ(s)) with suction.

to 0.92 MPa. A collapse of swelling pressure was observed after reaching the first peak. However, for the specimen hydrated by the vapour phase method (SP-01), no collapse was recorded in the evolution curve of swelling pressure. Explanations to these observations could be that, during the suction-controlled hydration process using the osmotic technique, water directly flows into the specimen through the large inter-pellet pores, leading to a rapid decrease of water potential in the macro-pores (inter-pellet pores). The collapse of swelling pressure may be attributed to the destruction of the capillary inter-granular forces induced by the wetting. However, for the specimen hydrated by the vapour equilibrium technique, water was slowly transferred into bentonite pellets and the water potential between the macro-pores and micro-pores remains essentially equal (Hoffmann et al., 2006). The inter-granular capillary forces changed slowly and no collapse was induced. As suction further decreased to lower values of 0.17 MPa and 0 MPa, hydration caused continuous increases of the swelling pressure. During this process, the clogging of large inter-pellet pores has almost completed and the granular structure of specimen disappears. The swelling pressure of specimen was mainly governed by the osmotic swelling.

5.1.3. Swelling deformation of GMZ bentonite pellet mixture

Under constant vertical stresses, the swelling of pellets upon hydration mainly contributes to the filling of large inter-pellet pores and the overall volume changes of the specimen. At the initial hydration stage (from 113 MPa to 38 MPa), the crystalline swelling dominated the expansion of bentonite pellets. The hydration of pellets induced the overall swelling of specimens (SD-01 and SD-08) under low vertical stresses. However, under the high vertical stresses, a collapse was observed in the specimen SD-09 (Fig. 7). This phenomenon indicated that, under the high vertical stresses, the suction-controlled hydration process by the vapour equilibrium technique also induced the collapse of granular structure. This collapse might be attributed to the rearrangement of pellets induced by wetting.

As suction further decreased to 4.2 MPa, the corresponding void ratio of the specimen SD-08 was close to its initial value. This phenomenon indicated that, during the step-by-step hydration (from 113 MPa to 4.2 MPa), the swelling of pellets mainly contributed to the filling of large inter-pellet pores. Once specimens were wetted by injecting liquid water or the osmotic technique, void ratios of specimens significantly increased, which were sensitive to the vertical stresses (Fig. 7). At the low suction stage (< 4.2 MPa), the swelling of pellet upon hydration was mainly dominated by the osmotic swelling. Since the filling of inter-pellet pores was almost completed, further hydration of the specimen led to significant swelling of the specimen. Furthermore, the increase of vertical stresses reduced the swelling strains of specimens through limiting development of diffuse double layers.

5.2. Compressibility properties of GMZ bentonite pellet mixtures

The unloading curves of specimens SD-06 and SD-07 in the compression tests exhibited a nearly bi-linearity, which was consistent to that recorded on a Ypresian clay by Cui et al. (2013). This phenomenon could be attributed to the competition between the mechanical and physico-chemical effects. The mechanical effect refers to the elastic

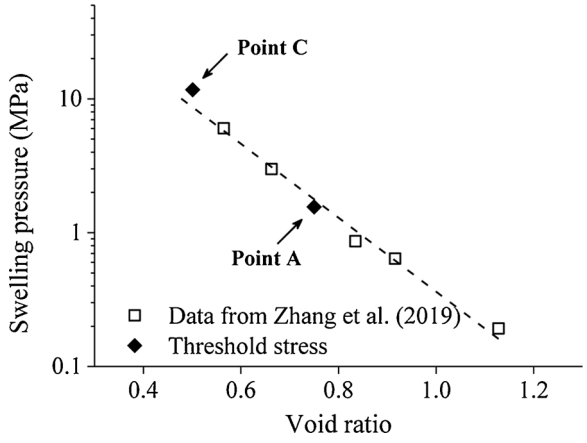

Fig. 12. Relationship between swelling pressure and void ratio.

deformation of soil particles, while the physico-chemical effect is the interaction between clay particles and adsorbed water. For a saturated clayey soil, upon mechanical loading, more and more orientated particles are generated and the physico-chemical effect is enhanced (Le et al., 2011). When the external stress is higher than the repulsive force related to the soil particle-water interaction (physico-chemical effect), low rebound deformation can be recorded on unloading. However, when the external stress is lower than the repulsive force, the prevailing physico-chemical effect causes a significant microstructural change by the formation of more and more face-to-edge particle contacts (Cui et al., 2013). Consequently, apparent rebound deformations can be observed in Fig. 9b when the vertical pressures are lower than the threshold stresses (σ_A and σ_C). However, the unloading curves are almost linear for specimens SCC-01, SD-01 and SD-02 (Fig. 9a). This can be interpreted that, at the high suction stage, less orientated particles during loading were generated and the unloading behavior was mainly dominated by the mechanical effect. Meanwhile, points A and C in Fig. 9b agree well with the relationship between the swelling pressure and void ratio (Fig. 12) developed by Zhang et al. (2019).

Curves in Fig. 10 show that, at the zero suction, a good coincidence can be observed in the preconsolidation pressures of the pellet mixture and the compacted bentonite powder. However, for non-zero suctions, the preconsolidation pressure of compacted bentonite powder significantly increases with increasing suction, while only a slight increase can be observed for the bentonite pellet mixtures. At the high suction stage, the inter-pellet pores in the mixture specimen has not completely disappeared. During the mechanical loading, the rearrangements and the crushing of pellets could occur, resulting in the significant compression in inter-pellet pores. But at the zero suction, the mixture specimen completely lost its granular structure and the inter-pellet pores almost all disappeared and the pore structure of the mixture is similar to that of compacted bentonite powder, resulting in comparable preconsolidation pressures.

Meanwhile, the swelling pressure (point B in Fig. 9b) obtained by the swell-consolidation method is higher than that obtained by the constant-volume method. Explanations could be that, with the swell-consolidation method, the specimen was firstly wetted under a low vertical load leading to a sufficient microstructural swelling and a significant swelling strain. Consequently, a higher vertical stress was needed to compensate this large swelling deformation.

6. Conclusion

In this work, suction controlled swelling pressure tests, swelling deformation tests and compressibility tests were conducted and the mechanical behavior of GMZ bentonite pellet mixtures over a wide suction range was investigated. Main conclusions can be drawn as follows.

For the specimen hydrated with suction-control by the vapour equilibrium technique, no collapse was observed on the evolution curve of swelling pressure. However, for the specimen wetted using the osmotic technique, the swelling pressure curve exhibited a bi-modal shape with a collapse observed after the first peak value reached. These observations could be explained by the bi-modal micro-structures and the hydration mechanisms with vapor infiltration and liquid water flooding of the compacted GMZ bentonite pellet mixtures.

For specimens hydrated with suction-control in a step-by-step way, a collapse was only observed on the swelling strain evolution curve under high vertical stresses, indicating the swelling of the pellet mixture specimens is sensitive to the applied vertical stress.

The unloading curves of specimens exhibited a linearity in high suction stage and a bi-linearity in low suction stage. The swelling pressure determined by the swell-consolidation method was higher than that determined by the constant-volume method.

Declaration of Competing Interest

No conflict of interest exits in the submission of the manuscript “Mechanical behavior of GMZ bentonite pellet mixtures over a wide suction range”. The manuscript was approved by all authors for publication. I would like to declare on behalf of my co-authors that the work described was original research that has not been published previously and not under consideration for publication elsewhere, in whole or in part.

Acknowledgements

The financial supports of the National Nature Science Foundation of China (41527801, 41672271 and 41807237) and the Shanghai Pujiang Program (18PJ1410200) are greatly acknowledged.

References

Alonso, E.E., Romero, E., Hoffmann, C., 2011. Hydromechanical behaviour of compacted granular expansive mixtures: experimental and constitutive study. Geotechnique 61 (4), 329–344.
Blatz, J.A., Cui, Y.J., Oldecop, L., 2008. Vapour equilibrium and osmotic technique for suction control. Geotech. Geol. Eng. 26 (6), 661–673.
Cui, Y.J., Tang, A.M., Qian, L.X., Ye, W.M., Chen, B., 2011. Thermal-mechanical behavior of compacted GMZ bentonite. Soils Found. 51 (6), 1065–1074.
Cui, Y.J., Nguyen, X.P., Tang, A.M., Li, X.L., 2013. An insight into the unloading/reloading loops on the compression curve of natural stiff clays. Appl. Clay Sci. 83-84, 343–348.
Darde, B., Tang, A.M., Pereira, J.M., Roux, J.N., Dangla, P., Talandier, J., Vu, M.N., 2018. Hydro-mechanical behaviour of high-density bentonite pellet upon partial hydration. Géotechniq. Lett. 8 (4), 1–23.
Delage, P., Howat, M.D., Cui, Y.J., 1998. The relationship between suction and swelling properties in a heavily compacted unsaturated clay. Eng. Geol. 50 (1–2), 31–48.
Dixon, D., Sanden, T., Jonsson, E., Hansen, J., 2011. Backfilling of Deposition Tunnels: Use of Bentonite Pellets. SKB P-11-44, Stockholm, 52 pp.. .
Gens, A., Alonso, E.E., 1992. A framework for the behaviour of unsaturated expansive clays. Can. Geotech. J. 29, 1013–1032.
Hoffmann, C., Alonso, E.E., Romero, E., 2007. Hydro-mechanical behaviour of bentonite pellet mixtures. Phys. Chem. Earth Parts A/b/c 32 (8), 832–849.
Hoffmann, C., Alonso, E.E., Romero, E., 2006. Fabric changes of a pellet-based bentonite buffer material and its effect on mechanical behaviour. Geotech. Spec. Publ. 2 (147), 2523–2534.
Imbert, C., Villar, M.V., 2006. Hydro-mechanical response of a bentonite pellets/powder mixture upon infiltration. Appl. Clay Sci. 32 (3–4), 197–209.
Komine, H., 2004. Simplified evaluation on hydraulic conductivities of sand–bentonite mixture backfill. Appl. Clay Sci. 26 (1–4), 13–19.
Le, T.T., Cui, Y.J., Muoz, J.J., Delage, P., Tang, A.M., Xiangling, L.I., 2011. Studying the stress-suction coupling in soils using an oedometer equipped with a high capacity tensiometer. Front. Struct. Civ. Eng. 5 (2), 160–170.
Lloret, A., Villar, M.V., Sanchez, M., Gens, A., Pintado, X., Alonso, E.E., 2003. Mechanical behaviour of heavily compacted bentonite under high suction changes. Geotechnique 53 (1), 27–40.
Lloret, A., Villar, M.V., 2007. Advances on the knowledge of the thermo-hydro-mechanical behaviour of heavily compacted “FEBEX” bentonite. Phys. Chem. Earth Parts A/b/c 32 (8-14), 0–715.
P. Marjavaara , E. Holt , P. Rantamäki , P. Oy . Customized bentonite pellets–extrusion manufacturing and gap filling & thermal performance properties–14262 Phoenix,

Arizona, USA WM2014 Conference vol. 1 2014.
Massat, L., Cuisinier, O., Bihannic, I., Claret, F., Pelletier, M., Masrouri, F., 2016. Swelling pressure development and inter-aggregate porosity evolution upon hydration of a compacted swelling clay. Appl. Clay Sci. 124-125, 197–210.
Molinero-Guerra, A., Mokni, N., Delage, P., Cui, Y.J., Tang, A.M., Aimedieu, P., 2017. In-depth characterisation of a mixture composed of powder/pellets MX-80 bentonite. Appl. Clay Sci. 135 (2016), 538–545.
Molinero-Guerra, A., Aimedieu, P., Bornert, M., Cui, Y.J., Tang, A.M., 2018. Analysis of the structural changes of a pellet/powder bentonite mixture upon wetting by X-ray computed microtomography. Appl. Clay Sci. 165, 164–169.
Mooney, R.W., Keenan, A.G., Wood, L.A., 1952. Adsorption of water vapor by montmorillonite. ii. effect of exchangeable ions and lattice swelling as measured by X-ray diffraction. J. Am. Chem. Soc. 74 (6), 1371–1374.
Pestana, J.M., Whittle, A.J., 1995. Compression model for cohesionless soils. Geotechnique 45, 611–631.
Posiva, 2010. TKS-2009. Nuclear Waste Management at Olkiluoto and Loviisa Power Plants. Review of Current Status and Future Plans for 2010–2012. Posiva Oy, Finland.
Romero, E., Gens, A., Lloret, A., 2003. Suction effects on a compacted clay under non-isothermal conditions. Geotechnique 53 (1), 65–81.
Romero, E., Villar, M.V., Lloret, A., 2005. Thermo-hydro-mechanical behaviour of two heavily over-consolidated clays. Eng. Geol. 81 (3), 255–268.
Saiyouri, N., Hicher, P.Y., Tessier, D., 2000. Microstructural approach and transfer water modelling in highly compacted unsaturated swelling clays. Mech. Cohes. Frict. Mater. 5, 41–60.
Saiyouri, N., Tessier, D., Hicher, P.Y., 2004. Experimental study of swelling in unsaturated compacted clays. Clay Miner. 39 (4), 1–11.
SKB, 2007. Fud-program 2007. Program för forskning, utveckling och demonstration av metoder för hantering och slutförvaring av kärnavfall. Svensk Kärnbränslehantering AB (In Swedish). .
Sugita, Y., Suzuki, H., Chijimatsu, M., 2003. Thermal, hydraulic and swelling properties of bentonite pellet- examine on calculating parameter assessment on PRP. Research document. Plant Ecol. 33 (33), 43–49.
Tang, A.M., Cui, Y.J., 2007. Controlling suction by the vapour equilibrium technique at different temperatures, application to the determination of the water retention properties of MX80 clay. Can. Geotech. J. 42 (1), 287–296.
Van Geet, M., Volckaert, G., Roels, S., 2005. The use of microfocus x-ray computed tomography in characterising the hydration of a clay pellet/powder mixture. Appl. Clay Sci. 29 (2), 73–87.
Van Olphen, H., 1977. An introduction to clay colloid chemistry for clay technologists, geologists, and soil scientists. Science 143.
Villar, M.V., Lloret, A., 2004. Influence of temperature on the hydro-mechanical behaviour of a compacted bentonite. Appl. Clay Sci. 26 (1-4), 337–350.
Wang, Q., Tang, A.M., Cui, Y.J., Delage, P., Barnichon, J.D., Ye, W.M., 2013. The effects of technological voids on the hydro-mechanical behaviour of compacted bentonite–sand mixture. Soils Found. 53 (2), 232–245.
Wen, Z.J., 2006. Physical property of China's buffer material for high-level radioactive waste repositories. Chin. J. Rock Mech. Eng. 25 (4), 794–800.
Ye, W.M., Cui, Y.J., Qian, L.X., Chen, B., 2009. An experimental study of the water transfer through confined compacted GMZ bentonite. Eng. Geol. 108 (3-4), 169–176.
Ye, W.M., Chen, Y.G., Chen, B., Wang, Q., Wang, J., 2010. Advances on the knowledge of the buffer/backfill properties of heavily-compacted GMZ bentonite. Eng. Geol. 116 (1-2), 12–20.
Ye, W.M., Zhang, Y.W., Chen, B., Zheng, Z.J., Chen, Y.G., Cui, Y.J., 2012. Investigation on compression behaviour of highly compacted GMZ01 bentonite with suction and temperature control. Nucl. Eng. Des. 252, 11–18.
Zhang, Z., Ye, W.M., Liu, Z.R., Chen, B., Cui, Y.J., 2018. Influences of PSD curve and vibration on the packing dry density of crushed bentonite pellet mixtures. Constr. Build. Mater. 185, 246–255.
Zhang, Z., Ye, W.M., Liu, Z.R., 2019. Investigation of swelling behaviors of GMZ bentonite pellet mixtures. The 7th Asia-Pacific Conference on Unsaturated Soils.
Zhu, C.M., Ye, W.M., Chen, Y.G., Chen, B., Cui, Y.J., 2013. Influence of salt solutions on the swelling pressure and hydraulic conductivity of compacted GMZ01 bentonite. Eng. Geol. 166 (10), 74–80.